BOREAS An international journal of Quaternary research

Luminescence dating of lacustrine sediments from Tangra Yumco (southern Tibetan Plateau) using post-IR IRSL signals from polymineral grains

HAO LONG, TORSTEN HABERZETTL, SUMIKO TSUKAMOTO, JI SHEN, THOMAS KASPER, GERHARD DAUT, LIPING ZHU, ROLAND MÄUSBACHER AND MANFRED FRECHEN

BOREAS

Long, H., Haberzettl, T., Tsukamoto, S., Shen, J., Kasper, T., Daut, G., Zhu, L., Mäusbacher, R. & Frechen, M.: Luminescence dating of lacustrine sediments from Tangra Yumco (southern Tibetan Plateau) using post-IR IRSL signals from polymineral grains. *Boreas*. 10.1111/bor.12096. ISSN 0300-9483.

Radiocarbon dating of bulk organic matter is the most commonly used method for establishing chronologies of lake sediments for palaeoclimate reconstructions on the Tibetan Plateau. However, this method is likely to be problematic because the dated material often suffers from old carbon contamination. Recently, advances in luminescence-based chronological techniques have provided new options for dating lacustrine sediments. In the current study, we tested for the first time the applicability of a new post-IR IRSL (pIRIR) measurement protocol for dating fine-grained polymineral material from a deep-lake sediment core from the central part of Tangra Yumco, on the southern Tibetan Plateau. Our results show that: (i) radioactive disequilibria in the uranium decay chain were observed in the studied lake sediments, and thus taken into account for dose rate calculation by using a dynamic modelling approach; (ii) the suitability and robustness of the pIRIR protocol measured at 150°C ($pIRIR_{150}$) for our samples are confirmed by a set of luminescence characteristic tests as well as the agreement with an independent age control; (iii) turbidite deposition partly caused an insufficient resetting of luminescence signals and thus apparent overestimation in luminescence dating; (iv) compared with the luminescence-based age-depth model, the ^{14}C ages of bulk organic matter from the studied core generally yielded an age difference of ~2 ka, which is attributed to hardwater reservoir effects in Tangra Yumco. This study highlights the need for multi-dating approaches of lake sedimentary archives on the Tibetan Plateau.

Hao Long (longhao@niglas.ac.cn, lzugeolh@gmail.com), State Key Laboratory of Lake Sciences and Environment, Nanjing Institute of Geography and Limnology, Chinese Academy of Sciences (NIGLAS), 210008 Nanjing, China, and Leibniz Institute for Applied Geophysics (LIAG), Geochronology and Isotope Hydrology, 30655 Hannover, Germany; Torsten Haberzettl, Thomas Kasper, Gerhard Daut and Roland Mäusbacher, Physical Geography, Institute of Geography, Friedrich-Schiller-University Jena, 07743 Jena, Germany; Sumiko Tsukamoto and Manfred Frechen, Leibniz Institute for Applied Geophysics (LIAG), Geochronology and Isotope Hydrology, 30655 Hannover, Germany; Ji Shen, State Key Laboratory of Lake Sciences and Environment, Nanjing Institute of Geography and Limnology, Chinese Academy of Sciences (NIGLAS), 210008 Nanjing, China; Liping Zhu, Institute of Tibetan Plateau Research, Chinese Academy of Sciences, 100101 Beijing, China; *received 17th September 2013, accepted 30th June 2014.*

There are over 1000 lakes (larger than 1 km^2) distributed across the Tibetan Plateau (TP; Wang & Dou 1998). These can provide quantitative sediment archives for deciphering spatial and temporal patterns of past climate change. Many of these lakes yield high-quality palaeoclimate records for the Lateglacial and Holocene, but there are still disagreements and uncertainty concerning the spatial and temporal patterns of past climate changes, and the associated forcing mechanisms (Hou *et al*. 2012). Accurate and reliable dating of lacustrine deposits is of crucial importance in both the reconstruction of palaeolake/palaeoclimate evolution and the understanding of the mechanisms of climate changes (Long *et al*. 2011). Radiocarbon dating has been the most commonly used method for establishing chronologies of lake sediments (Walker 2005). However, environmental and climate reconstructions based on lake records from relatively dry and cold regions such as the TP are commonly hampered by the sparse terrestrial vegetation in the catchments and the resulting lack of terrestrial plant remains in lake sediments suitable for radiocarbon dating (Mischke *et al*. 2013). Thus, bulk organic matter has been routinely used for radiocarbon dating, which can be problematic because these bulk sediments often suffer from contamination from sources of 'old carbon' (carbon reservoir effect). The approaches commonly used to estimate the reservoir effect for TP lakes have been (i) to determine the radiocarbon ages of a lake sediment surface sample or core-top sample (Kasper *et al*. 2012; Mischke *et al*. 2013), or (ii) linear extrapolation of core age-depth data up to the lake sediment surface (Mügler *et al*. 2010; Hou *et al*. 2012). However, the first method does not take into account the post-bomb radiocarbon in the atmosphere during the period of sediment accumulation although ^{14}C levels have been significantly higher in recent decades in comparison to the atmospheric ^{14}C activity in 1950 used for reporting of radiocarbon dating results (Hua 2009). For the second method, the assumption that the sediment accumulation rates remain constant close to the sediment–water interface may often be inappropriate because of significant variations in sediment water content and organic matter degradation (Mischke *et al*. 2013). Further-

DOI 10.1111/bor.12096

more, both methods assume a constant reservoir effect and thus do not consider its variability through time. Our recent work suggested that carbon reservoir effects may be variable through time on long time scales in a lake sedimentary succession (Long *et al.* 2012a). As a result, it is difficult to assess the lake reservoir effect accurately in the TP lakes because of its variability in different lakes and even at different sites within individual lakes (Kasper *et al.* 2012; Mischke *et al.* 2013).

Lake reservoir effects can either be assessed or ignored if independent age data are available (e.g. Long *et al.* 2011; Rades *et al.* 2013). Over the past one and a half decades, advances in luminescence dating have provided a new chronological tool for lacustrine sediments (Haberzettl *et al.* 2009; Lang & Zolitschka 2001; Long *et al.* 2011 and references therein; Lukas *et al.* 2012; Shanahan *et al.* 2013). Recently, numerous studies have been published describing the use of this dating technique on many types of lake deposits from the TP and adjacent areas. For instance, Lee *et al.* (2011) and Long *et al.* (2011) applied coupled radiocarbon and optically stimulated luminescence (OSL) dating to quartz in shallow lake sediments from the northern foreland of the TP. They suggested that when aeolian processes are the dominant means of sediment deposition, especially in lakes of arid environments, OSL dating is superior to radiocarbon dating. In order to reconstruct lake evolution since the Late Pleistocene, quartz OSL proved to be a very robust dating technique in lake beach/terrace sediments from the TP (e.g. Madsen *et al.* 2008; Lee *et al.* 2009; Long *et al.* 2012b). However, there are few luminescence dating studies of lacustrine records from deep lakes in this area. The aim of the current study was to test the applicability of luminescence techniques in dating late Holocene deep-lake sediments, which could provide the opportunity to independently test other chronologies.

In the last decade, quartz has generally been considered as the preferred dosimeter in luminescence dating of Holocene sediments (Murray & Olley 2002; Madsen & Murray 2009). However, quartz OSL with low sensitivity exists in several parts of the world, particularly where the quartz grains have only recently been released from the source rock (Preusser *et al.* 2009). Such quartz mineral is not suitable for luminescence dating because of the dim OSL signal, especially for young samples (<10 ka), which results in a poor signal to noise ratio and thus a broad distribution of equivalent doses (D_es; e.g. Davids *et al.* 2010). By contrast, coarse grain (CG) (e.g. 100–200 μm) K-rich feldspar minerals could provide very bright and reproducible infrared-stimulated luminescence (IRSL) signals from samples for which quartz produces nearly undetectable OSL signals (e.g. Madsen *et al.* 2011). However, the single greatest factor that has prevented the widespread uptake of luminescence dating using feldspar is the phenomenon of anomalous fading (Wintle 1973). Anomalous fading is the decay of an unstable luminescence signal, which, if uncorrected, leads to an underestimation of the true age of the sample. Although a number of methods has been proposed to measure the rates of anomalous fading (Aitken 1985) and to correct for anomalous fading (Huntley & Lamothe 2001; Lamothe *et al.* 2003), all correction models have several inherent assumptions (e.g. Morthekai *et al.* 2008) and thus there has been no universally agreed model owing to its complexity.

Recently, advances have been achieved in isolating a luminescence signal from feldspar, which is less affected by anomalous fading. Thomsen *et al.* (2008) first reported that the IRSL signal observed at an elevated temperature (here called post-IR IRSL signal, abbreviated pIRIR) following a prior infrared (IR) stimulation at 50°C is more stable and has a much lower fading rate than the conventional IRSL signal measured at 50°C (abbreviated $IRSL_{50}$) for the same CG feldspar samples. Thereafter, an increasing number of methodological studies as well as dating applications have been presented using this new protocol for CG feldspar from different kinds of sediments, suggesting the protocol to be very promising, although it was mainly developed for old samples (i.e. beyond ~100 ka). The pIRIR protocol was also applied on polymineral fine grains (4–11 μm, FG) from loess samples (e.g. Buylaert *et al.* 2011; Stevens *et al.* 2011; Thiel *et al.* 2011; Roberts 2012). Due to strong thermal quenching and the low cross-section of quartz to IR, the IRSL signal of the 4–11 μm fraction at elevated temperature is completely dominated by luminescence from feldspars (Buylaert *et al.* 2012), especially from Na-rich feldspar (Tsukamoto *et al.* 2012). Buylaert *et al.* (2012) summarized the $pIRIR_{290}$ ages derived from CG K-feldspar extracts or FG polymineral from a variety of sedimentary samples around the world; by comparison with the independent ages, they confirmed the robustness of the used dating protocol without fading correction. However, the pIRIR signal may give rise to a large residual dose. For instance, Buylaert *et al.* (2012) reported residual doses of ~4–5 Gy from the $pIRIR_{290}$, which did not affect their old samples but are of significant importance for younger deposits. A set of modified pIRIR protocols (e.g. with stimulation temperature of 150°C and a preheat temperature of 180°C) were tested for Holocene coastal sediments and showed that the residual doses vary from 0.05–0.8 Gy (Madsen *et al.* 2011; Reimann *et al.* 2011; Reimann & Tsukamoto 2012). More recently, this protocol was also applied for dating Holocene aeolian sediments using K-feldspar (Long *et al.* 2014). These attempts for the Holocene sediments were carried out only for CG K-feldspar minerals, but have not been tested for polymineral fine grains. The sediment from deep lakes mainly consists of fine grains. In the current study, the newly proposed post-IR IRSL protocol discussed

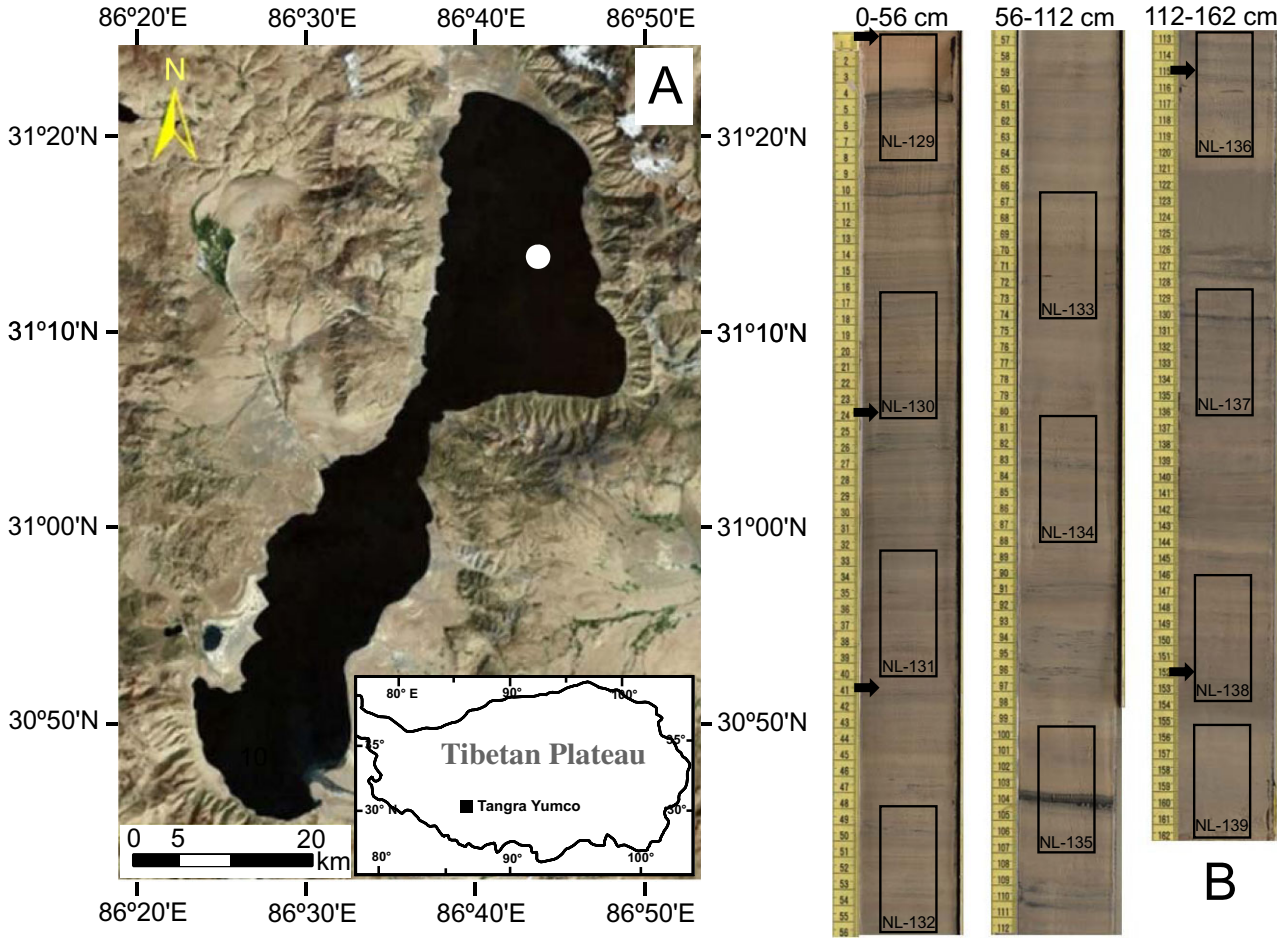

Fig. 1. A. Location of the studied sediment core (white dot) in Tangra Yumco and the location of this lake on the Tibetan Plateau (inset). B. Photographs showing the lithology of the TAN10/4 core, and sampling locations for luminescence dating (marked by rectangles) and ^{14}C dating (marked by arrows). This figure is available in colour at http://www.boreas.dk.

above was first tested using polymineral FG samples from a lake sediment core from Tibet. Subsequently the luminescence dating results were compared with an independent ^{14}C age control that is unrelated to any other luminescence method.

Study area and samples

Lake Tangra Yumco (latitude 30°45′–31°22′N, longitude 86°23′–86°49′E, altitude 4528 m a.s.l.) is located in the southern part of the TP (inset in Fig. 1A). This lake is a closed basin (Fig. 1A) with a surface area of 818 km^2 and a drainage area of 8219 km^2. Several streams, mainly from the west and south, drain into Tangra Yumco. A 162-cm-long gravity core, TAN10/4 (31°15′9.54″N, 86°43′22.14″E), was retrieved from the deepest area (water depth: 223 m, Wang *et al.* 2010) in the centre of the northern lake basin (Fig. 1A). Its main lithology is partly fine-laminated (1–5 mm), greyish silty clay with intercalated dark brownish to blackish fine sand layers (Fig. 1B). This main deposit is interrupted by four layers probably originating from abrupt sedimentation events (e.g. turbidites). After core splitting, one half was used for collecting luminescence dating material. Under the condition of subdued red light, the inner non-light-exposed part was collected for D_e determination; the outer ~1 cm (potentially bleached material of this core) was taken for dose rate measurements. Eleven samples were obtained for luminescence dating (Fig. 1B), and five samples were collected for accelerator mass spectrometry (AMS) ^{14}C dating at Beta Analytic Inc. (Miami, Florida, USA).

Luminescence dating method

Sample preparation and equipment

The samples for D_e measurements were first wet sieved to obtain two fractions (>38 and <38 μm). The fraction of <38 μm was treated with 10% HCl and 30% H_2O_2 to remove any carbonates and organic matter. The FG

polymineral fraction was separated according to Stokes' law. It was initially intended to use FG quartz for luminescence dating. The prepared polymineral samples were etched by 30% H_2SiF_6 (hydrofluorosilicic acid) for 3–4 days to obtain pure FG quartz extracts. Unfortunately, the quartz OSL signal intensity was too low to be detected (see below), suggesting that OSL dating may be impractical for routine use. Therefore, we used the IRSL signal from polymineral FG, which is dominated by luminescence emissions from feldspar, applying the pIRIR protocol for dating. Using deionized water, about 1 mg of each obtained polymineral FG or quartz sample was settled on an aluminium disc for luminescence measurements.

D_e values were measured with an automated luminescence reader (Risø TL/OSL DA-15, Bøtter-Jensen *et al.* 2000) equipped with a $^{90}Sr/^{90}Y$ beta source. For the quartz OSL, blue LEDs (470 nm) were used for stimulating the aliquots and a 7.5-mm Hoya U-340 filter was used as the signal detection filter in front of the photomultiplier tube. For the IR stimulation of polymineral FG, infrared LEDs (870 nm) were used and the IRSL signal was detected through a combination of Schott BG-39 and Corning 7–59 filters in the blue light spectrum between 320 and 450 nm.

Measurement protocol for equivalent dose estimation

Based on the single-aliquot regenerative-dose (SAR) method (Murray & Wintle 2000), the applicability of an elevated temperature pIRIR SAR protocol originally proposed by Thomsen *et al.* (2008) was tested. Recently, Madsen *et al.* (2011) and Reimann *et al.* (2011) modified and applied this protocol for dating coastal sands of Holocene age, for which independent age control was available. The pIRIR SAR protocol (Table 1) applied in this study includes the measure of a low temperature IRSL signal at 50°C ($IRSL_{50}$) as well as an IR signal at an elevated temperature (at 150°C, $pIRIR_{150}$) after the $IRSL_{50}$ for dating young lake sediments following Reimann & Tsukamoto (2012). For the first SAR cycle, which measures the natural dose built up by the radiation field present in the natural environment, no laboratory dose was administered. In the next step of the SAR cycle, a beta dose was given (step 1). Samples were then preheated for 60 s at 180°C (step 2), followed by an IR stimulation at 50°C for 100 s (step 3) and a second IR stimulation for 200 s by holding the sample temperature at 150°C (step 4); here the luminescence (L_i) was measured. Correction for sensitivity changes throughout the measurement cycle was carried out by application of a test dose (step 5) as part of the SAR procedure. The test dose (~6.1 Gy) signal was measured in a similar manner; the samples were first heated to 180°C (step 6) and then stimulated by IR diodes for 100 s at 50°C (step 7) followed by an IR stimulation for 200 s at 150°C (step 8) during which the test dose response (T_i) was measured. In practice, L_i and T_i were calculated using both the $IRSL_{50}$ and $pIRIR_{150}$ signals, in order to allow a comparison of the behaviour of the two signals (L_i and T_i of the $IRSL_{50}$ were measured in steps 3 and 7, respectively). For both the $pIRIR_{150}$ and $IRSL_{50}$ signals the integrated signal was calculated from the initial 10 s, less a background derived from the last 10 s.

Table 1. Modified $pIRIR_{150}$ protocol used for equivalent dose determination.

Step	Treatment	Observed
1	Dose	
2	Preheat at 180°C for 60 s	
3	IRSL measurement at 50°C for 100 s	Lx1
4	IRSL measurement at 150°C for 200 s	Lx2
5	Test dose	
6	Preheat at 180°C for 60 s	
7	IRSL measurement at 50°C for 100 s	Tx1
8	IRSL measurement at 150°C for 200 s	Tx2
9	Return to step 1	

Dose rate determination

Part of the sampled material from sediment core TAN10/4 was used for the measurement of water content and dose rate. Water contents were calculated by weighting the sediments before and after drying at 50°C for 3 days, with the weight loss expressed as a percentage of dry weight (10% error). The specific activities of radionuclides were measured by high-resolution gamma spectrometry (Murray *et al.* 1987). The radionuclide concentrations (U, Th and K content) of the surrounding sediment were also measured by neutron activation analysis (NAA). For the former method, the samples were dried at 130°C and ground for homogenization. Afterwards about 6 g of material for each sample was placed into a plastic container for measurements using a Well detector. The prepared samples were sealed and stored for 1 month to ensure equilibrium between ^{222}Rn and ^{226}Ra before determining the activities of natural U, ^{232}Th and their daughter nuclides and ^{40}K. Each sample was measured for 3–4 days. For submerged sediments (e.g. deep-lake sediments) disequilibrium in the ^{232}Th chain is rare because of the short half-lives of the ^{232}Th daughters, but it is relatively common for the ^{238}U chain (Olley *et al.* 1996), which may result in variable dose rate through burial time. In order to check if there are disequilibria in the current studied lake sediments, the activities of ^{238}U (obtained from ^{234}Th), ^{226}Ra (obtained from ^{214}Bi and ^{214}Pb, which are daughters of ^{226}Ra) and ^{210}Pb were compared. The cosmic dose contribution to the dose rate is negligible because the water depth of the core position is 223 m. Finally, the total dose rates were calculated using the conversion factors of Guérin *et al.* (2011).

Table 2. Summary of dosimetric information derived from gamma spectrometry analysis.

Sample	Sediment depth (cm)	^{238}U (Bq kg^{-1})	^{226}Ra (Bq kg^{-1})	^{210}Pb (Bq kg^{-1})	^{232}Th (Bq kg^{-1})	^{40}K (Bq kg^{-1})
NL-129	0–8	93.2±2.0	73.3±0.6	143.7±3.8	77.7±0.3	803.1±6.2
NL-130	16–24	107.9±2.2	77.7±0.4	87.3±2.1	79.1±0.3	802.9±8.8
NL-131	32–40	85.7±4.7	71.2±0.8	81.6±3.1	68.3±0.5	726.1±8.2
NL-132	48–56	102.7±4.3	84.9±0.7	86.3±3.9	77.0±0.4	835.2±8.3
NL-133	66–74	107.3±3.4	81.4±0.6	84.2±3.6	79.3±0.5	803.4±9.3
NL-134	80–88	114.0±4.4	75.3±0.6	81.7±4.3	78.0±0.5	819.3±7.7
NL-135	99–107	105.7±5.0	59.1±1.0	66.7±5.2	74.8±0.6	817.3±11.8
NL-136	112–120	120.4±3.2	69.7±0.5	75.3±2.8	75.6±0.4	778.6±6.8
NL-137	128–136	111.8±4.2	70.1±0.4	72.7±2.8	76.3±0.3	809.6±6.6
NL-138	146–154	108.0±6.4	68.1±0.8	66.7±4.3	80.7±0.6	847.0±10.1
NL-139	155–162	120.8±5.5	67.9±0.6	70.7±3.2	80.3±0.4	811.7±7.1

Results and discussion

Dosimetry

The activities of radionuclides are summarized in Table 2. The comparison of the activities of ^{238}U, ^{226}Ra, and ^{210}Pb are shown in Fig. 2A–C. Across the core, activities of ^{238}U were generally higher than those of ^{226}Ra (20–80%), and ^{210}Pb (5–70%), except for the surface sample NL-129, which was due to natural atmospheric fall-out of ^{210}Pb. The fall-out ^{210}Pb on surface sediments normally results in an excess of ^{210}Pb over ^{226}Ra. However, this excess is unlikely to affect dose rate determinations significantly because any excess of ^{210}Pb (half-life ~22 years) will decay away in <100 years after burial, and also because the dose rate derived directly from the decay of ^{210}Pb and its daughters is small (Olley *et al.* 1996; Madsen *et al.* 2005). Furthermore, it was observed that the Ra-deficit (i.e. difference of ^{238}U and ^{226}Ra activities) increases with depth (Fig. 3). There are two possible causes for the uranium disequilibrium, i.e. uptake of U through time, and loss of Th at deposition. These two assumptions have been modelled below to consider the impact of U disequilibrium on the dose rates of sediments.

The first assumption requires that the concentration of U has increased with time. This interpretation would also require a very large amount of U in groundwater and a very large degree of scavenging by precipitated carbonate, which is possible in Tangra Yumco as the measured carbonate content of sediment core TAN10-4 ranges from 23.4 to 44.1% with an average of 35.6% (unpublished data). If this is the case, the disequilibrium is caused by postdepositional uptake of U, and uranium is supposed to be continuously taken up from circulating groundwater enriched in U after initial deposition of the sample. Thus, the average dose rate for the burial period for U was calculated from the sum of the dose rate based on the ^{226}Ra activity (which indicates initial activity of all nuclides of the U decay chain) and dose rate originates from half of the measured U excess (assuming linear integration of ^{238}U uptake since deposition). The calculated dose rates using this model (model 1) are shown in Table 3.

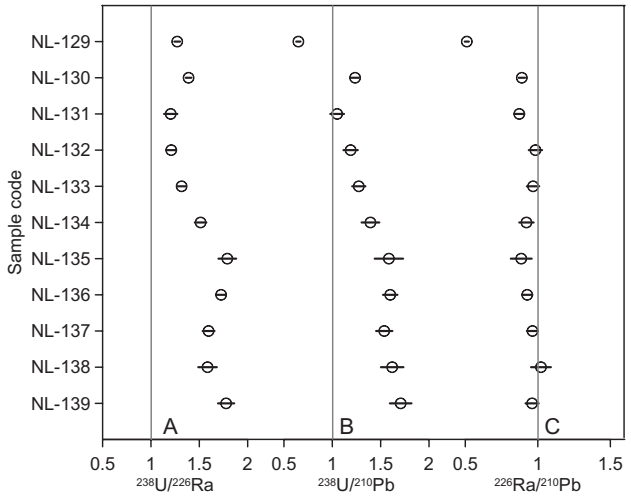

Fig. 2. Specific radionuclide activity ratios (A, B and C).

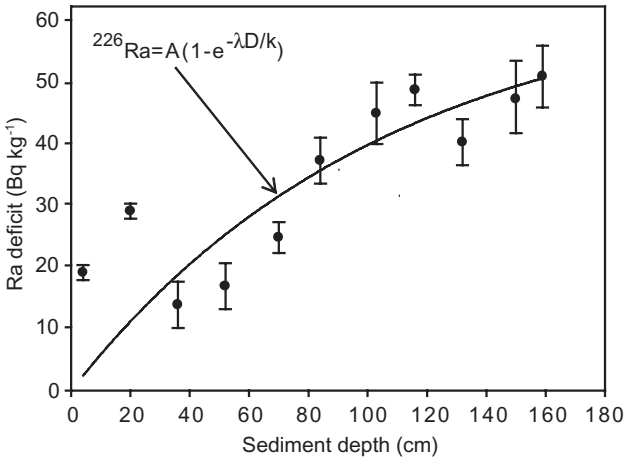

Fig. 3. Ra deficits (dots with error bars) for all samples fitted against depth with a saturating exponential function (solid curve).

Table 3. Results of dose rate determination by gamma spectrometry and NAA methods.

Sample	Sediment depth (cm)	U (ppm)		Th (ppm)		K (%)		Water content (%)	Total dose rate (mGy a^{-1})	
		Gamma[1]	NAA	Gamma	NAA	Gamma	NAA		Model 1	Model 2
NL-129	0-8	7.5 ± 0.54	6.42 ± 0.26	19.18 ± 1.05	17.30 ± 0.42	2.58 ± 0.15	2.21 ± 0.07	108 ± 10	3.21 ± 0.16	
NL-130	16-24	8.69 ± 0.6	7.71 ± 0.27	19.52 ± 1.07	18.70 ± 0.45	2.58 ± 0.16	2.29 ± 0.07	101 ± 10	3.48 ± 0.17	3.77 ± 0.22
NL-131	32-40	6.90 ± 0.51	6.98 ± 0.25	16.87 ± 0.97	16.00 ± 0.38	2.34 ± 0.14	2.23 ± 0.08	104 ± 10	2.98 ± 0.15	3.33 ± 0.20
NL-132	48-56	8.26 ± 0.58	7.46 ± 0.28	19.00 ± 1.07	17.20 ± 0.41	2.69 ± 0.16	2.06 ± 0.07	136 ± 10	2.94 ± 0.15	3.11 ± 0.18
NL-133	66-74	8.63 ± 0.60	7.53 ± 0.26	19.56 ± 1.11	16.60 ± 0.40	2.58 ± 0.16	2.05 ± 0.07	128 ± 10	3.04 ± 0.15	3.35 ± 0.20
NL-134	80-88	9.17 ± 0.62	7.68 ± 0.26	19.31 ± 1.09	15.90 ± 0.38	2.63 ± 0.16	2.06 ± 0.07	107 ± 10	3.39 ± 0.16	3.88 ± 0.24
NL-135	99-107	8.51 ± 0.59	7.48 ± 0.28	18.45 ± 1.09	16.90 ± 0.41	2.63 ± 0.17	2.08 ± 0.07	106 ± 10	3.21 ± 0.15	
NL-136	112-120	9.69 ± 0.65	8.71 ± 0.28	18.66 ± 1.03	16.40 ± 0.39	2.50 ± 0.15	2.09 ± 0.07	131 ± 10	2.93 ± 0.14	
NL-137	128-136	9.00 ± 0.61	8.29 ± 0.27	18.83 ± 0.95	16.30 ± 0.39	2.60 ± 0.15	2.07 ± 0.07	117 ± 10	3.14 ± 0.15	3.84 ± 0.24
NL-138	146-154	8.69 ± 0.60	7.83 ± 0.27	19.89 ± 1.16	17.70 ± 0.42	2.72 ± 0.15	2.15 ± 0.07	132 ± 10	3.00 ± 0.14	3.65 ± 0.22
NL-139	155-162	9.72 ± 0.65	8.15 ± 0.28	19.81 ± 1.00	17.90 ± 0.41	2.61 ± 0.15	2.11 ± 0.07	123 ± 10	3.14 ± 0.14	

[1]U content is derived from ^{234}Th.

The second assumption requires some prior ^{230}Th separation during sediment transportation and sedimentation. In such a case one would expect the ^{226}Ra to decay towards equilibrium with its parent ^{230}Th with a half-life of 1600 years. The effect of this explanation is shown in Fig. 3, where the Ra deficit is plotted as a function of depth, and the data fitted with a simple saturating exponential curve ($^{226}Ra = A(1-e^{-\lambda D/k})$); where A is the saturation value calculated by this exponential fitting; λ/k is the exponential constant, where λ is the ^{226}Ra decay constant, k is the sedimentation rate and D is the depth. The resulting value of A is 65 Bq kg^{-1}, and k was calculated to 0.045 cm a^{-1}, which fits the depositional rate based on the luminescence dates (see below). Thus, our data are consistent with the idea of ^{226}Ra decay towards equilibrium with its ^{230}Th parent.

^{226}Ra and its daughters account for about 75% of the dose rate from the ^{238}U decay chain at secular equilibrium (Olley *et al*. 1996); disequilibria that involve ^{226}Ra will therefore have a significant effect on the dose rate. Therefore, we need to take into account the variation in the dose rate derived from ^{226}Ra and daughters with time to obtain the correct age. The dose rate calculated from natural radionuclides is divided into three parts: the first one is the equilibrium part for Th, K and the supported part of U, and the supported U is obtained from parent U minus ^{230}Th, which was calculated from the fitting of Ra deficit with depth (Fig. 3); the second is the unsupported part only for ^{238}U, ^{234}Th, ^{234}Pa and ^{234}U, whose activities are larger than those of the rest of the daughters, and is calculated from the difference between the observed ^{226}Ra and the supported part; the last one is excess ^{226}Ra and its daughters, which was calculated iteratively, with the initial age estimates using the observed unsupported part. However, the actual activity of ^{226}Ra must have been higher during the burial time than the observed unsupported part. We thus used the initial age to estimate how much more Ra existed on average compared with the supported part, which was incorporated into the iterative calculation. The iteration was stopped after about three times, when no further significant changes in dose rates and ages occurred. The iterative calculations were not applied to samples NL-129, NL-135, NL-136 and NL-139 as their ages were significantly overestimated owing to partial bleaching (see below). The dose rate results calculated by this model (model 2) are shown in Table 3 and indicate that both models yielded similar dose rates for the sediment samples except for samples NL-129, NL-135, NL-136 and NL-139. We applied the dose rates derived from both models for the final age calculations.

The radionuclide concentrations of all 11 samples were also determined by the NAA method (Fig. 4; Table 3). The NAA results show a systematic tendency to underestimate the gamma spectrometry results in Th (~2 ppm) and K (~0.5%) (Fig. 4B, C). The average values of the two methods were used to calculate the contribution of Th and K to the natural dose rate. The U contents obtained by the NAA method are close to the results derived from ^{234}Th using gamma spectrometry (Fig. 4A), however, this method cannot detect U-series disequilibrium. Thus, it is improper to use the U values based on NAA analysis to calculate the dose rate for such an environment.

Considering that there is no evidence for systematic trends in water content with depth in the sediment core (Fig. 4D), we assumed negligible impacts of compaction on the water content of sediments from core TAN10/4. As a result, the measured water content,representing a minimum estimate, was used for luminescence age calculations.

Luminescence characteristics

Figure 5A shows two representative examples of decay curves from the FG quartz tests, showing a very low natural OSL signal. All 11 FG quartz samples showed

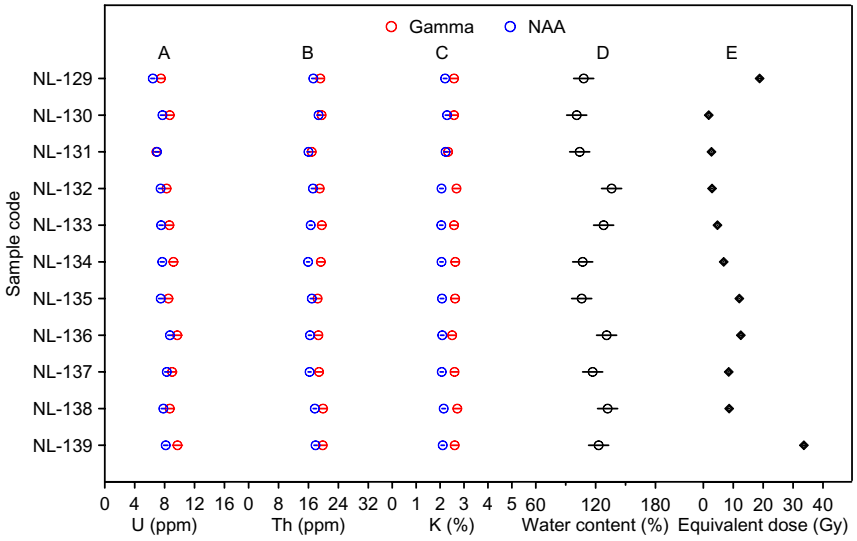

Fig. 4. Comparison of the radionuclide analyses (A, B and C), as well as measured water content (D) and equivalent dose (D_e, E). This figure is available in colour at http://www.boreas.dk.

very dim natural and regenerated OSL signals. Only several tens of counts for the first 0.16 s of stimulation were obtained when a test dose of ~6.1 Gy was applied. Thus, the quartz mineral was not considered to be suitable for luminescence dating in the current case. Subsequently we focused on the IRSL signal of polymineral FG for dating. In Fig. 5B an example for a natural $IRSL_{50}$ decay curve and the subsequently measured $pIRIR_{150}$ decay curve for one aliquot of sample NL-138, together with the dose response curves of both signals for the same aliquot, are shown.

It is commonly accepted that three routine tests should be carried out for any new SAR protocol used for equivalent dose determination, i.e. examination of the recycling ratio, recuperation and dose recovery (Murray & Wintle 2000; Buylaert *et al.* 2009). Figure 6A summarizes the recycling ratios for the $pIRIR_{150}$ signal, in which the sensitivity-corrected luminescence intensity observed from the first regenerative dose is divided by the corrected intensity observed when the same dose is repeated at the end of the SAR measurement sequence (Murray & Wintle 2000). The overall recycling ratio for all samples in this study is 1.020±0.003 (n = 126), illustrating that the sensitivity correction worked well and that the measurements taken following the laboratory irradiations are reproducible. Figure 6B summarizes the recuperation values, that is, the response to a zero-Gy laboratory dose, measured just after the SAR cycle for the natural dose. These signals are expressed as a percentage of the sensitivity-corrected natural luminescence. Recuperation for most of the measured aliquots was less than 10% and the average for all measured aliquots was 4.761±0.177% (n = 126) of the natural signal. This was considered acceptably small.

In order to further confirm the suitability of the measurement protocol used, dose recovery tests were undertaken for the 11 samples (three aliquots for each sample). First, the aliquots were bleached with a solar simulator (Hönle SOL2) lamp for 4 h (e.g. Reimann *et al.* 2011; Buylaert *et al.* 2012). They were then given a known dose of ~7.3 Gy and measured using the pIRIR protocol shown in Table 1. All data for the dose recovery tests of the 11 samples (33 discs in total) are presented in Fig. 7A, demonstrating that all measured-to-given dose ratios for $pIRIR_{150}$ signal are between 0.9 and 1.1 after subtracting the residual dose mentioned below. The mean dose-recovery ratio was 0.988±0.005. This suggests that our protocol is able to accurately measure doses given in the laboratory before heating and optical treatment. All these laboratory tests indicate that the overall behaviour of the SAR protocol when applied to the pIRIR signals from the samples appears to be satisfactory.

In addition, signal bleaching is of particular importance in luminescence dating of young samples. It is known that feldspar luminescence is bleached by daylight more slowly than the OSL from quartz (Murray *et al.* 2012 and references therein). Furthermore, elevated temperature IRSL bleaches more slowly than IRSL stimulated at low temperatures (Buylaert *et al.* 2012; Reimann & Tsukamoto 2012). Residual doses were measured using three aliquots for each sample after exposure to Hönle SOL2 for 4 h. The tests showed that the residual doses ranged between 0.2 and 0.8 Gy (Fig. 7B), resulting in possible age overestimation of approximately 80 to 250 a for the samples under study. These residual doses are much lower than those of the pIRIR signals measured at a much higher temperature. For instance, Buylaert *et al.* (2012) reported a residual dose of ~4–5 Gy (equivalent to ~2–3 ka) for the $pIRIR_{290}$ signal from modern samples. The current study suggests the effectiveness of reducing the residual dose by using a much lower preheat temperature of

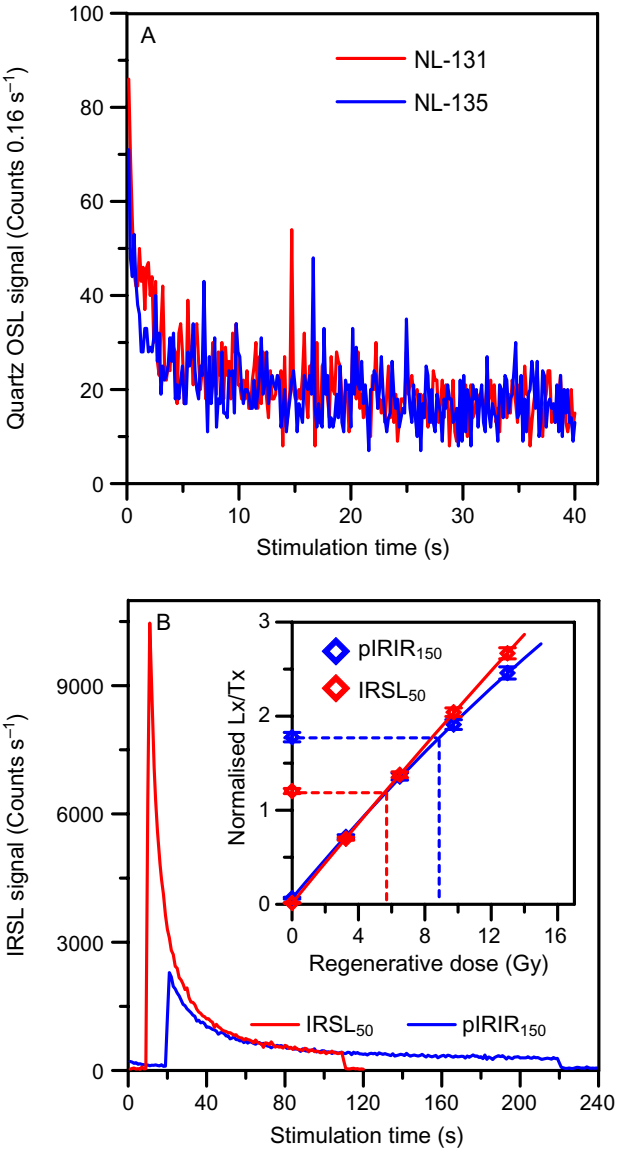

Fig. 5. A. Two example decay curves showing very low natural quartz OSL signals. B. Typical IRSL and pIRIR decay curves of FG polymineral and corresponding growth curves (inset) of sample NL-138. This figure is available in colour at http://www.boreas.dk.

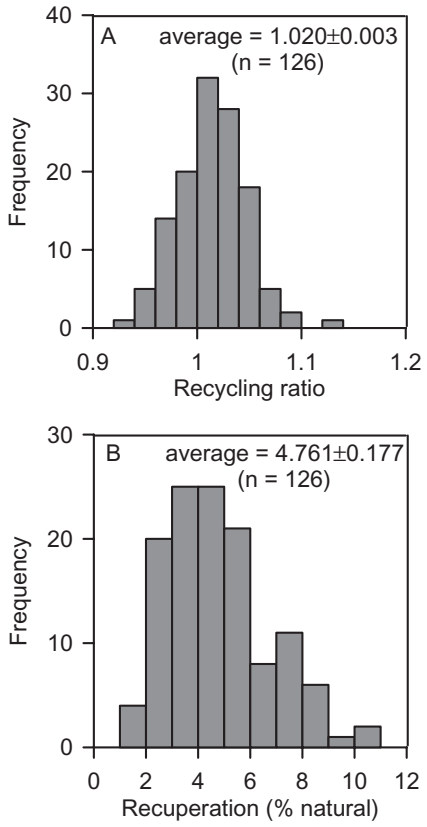

Fig. 6. Histograms summarizing the recycling ratios (A) and recuperation values (B) of pIRIR$_{150}$ measurements.

180°C and pIRIR stimulation at 150°C. These residual doses are comparable to the values (0.3–0.8 Gy) reported by Reimann & Tsukamoto (2012) for young (<500 a) coastal K-feldspar (CG fraction) from Germany, but much larger than observations (0.05–0.07 Gy) made by Madsen *et al.* (2011) and obtained from pIRIR$_{150}$ of modern coastal and aeolian sediments from New Zealand. It is noted that the residual doses are different from one another for the studied 11 samples and that there is a slight increasing trend with D_e (Fig. 7C). Considering that the residual dose is not negligible compared with the D_e values of the late Holocene sediments, the measured residual doses were subtracted from the measured D_e values for age calculation.

Fading tests

It is well known that most feldspar samples suffer from anomalous fading. Huntley & Lamothe (2001) showed that the luminescence signal decays linearly with the logarithm of time (t) and attributed this loss to anomalous fading. Anomalous fading is usually quantified by the *g*-value, which represents the signal loss per decade of normalized storage time. A dose similar to the natural dose of each sample was given by the beta source and the normalized luminescence was measured following various time delays. The pIRIR protocol described above (Table 1) was used to calculate *g*-values for the IRSL$_{50}$ and the pIRIR$_{150}$ using six aliquots for each sample. Preheat was conducted immediately following the irradiation, and thus prior to the delays (Auclair *et al.* 2003). The *g*-value of each aliquot was obtained by fitting a linear regression line to the sensitivity-corrected IRSL and pIRIR signals as a function of logarithmic normalized storage time (Fig. 8A). It shows a pronounced difference in the slopes of the fitted linear function between the two feldspar signals, which is equivalent to the *g*-value. Figure 8B shows the comparison of *g*-values for both IRSL$_{50}$ and pIRIR$_{150}$ signals derived from a representative sample (NL-130), ranging from 2.5±0.9 to 4.1±1.0%/decade and from 0.2±0.9 to 0.8±1.0 %/decade, respectively.

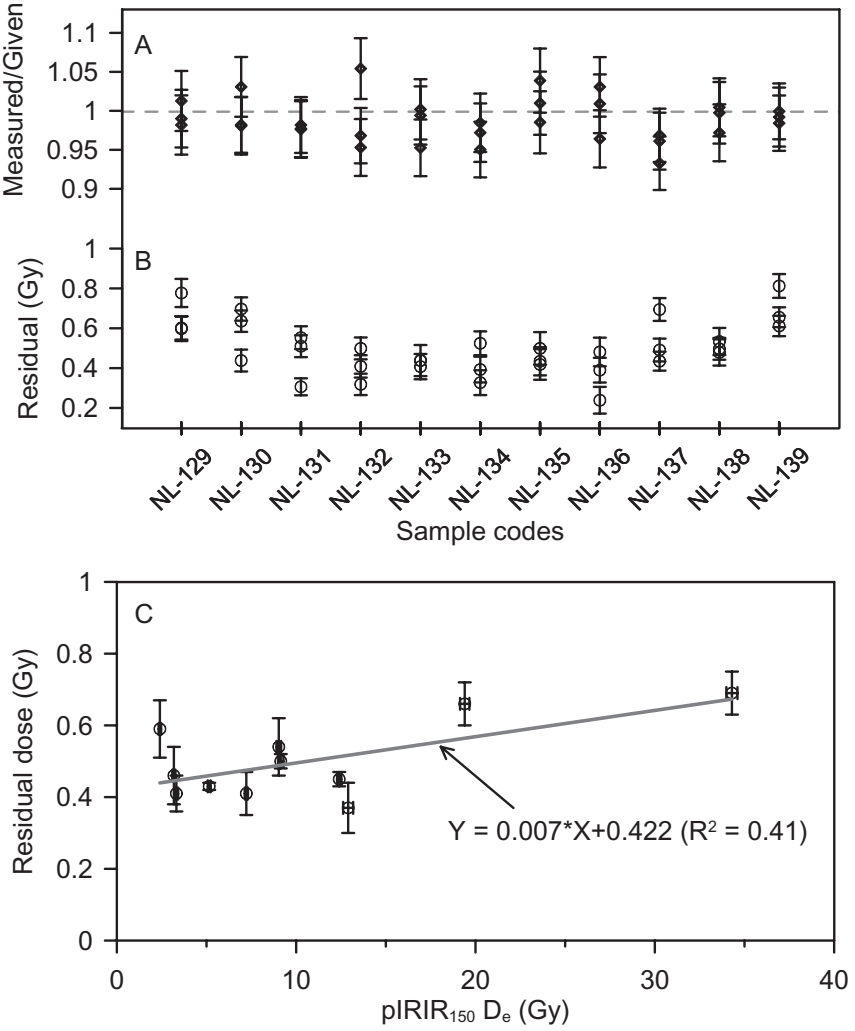

Fig. 7. Dose recovery ratio (A) and residual dose (B) on $pIRIR_{150}$ signal for the 11 samples (three discs were used for every test for each sample), and residual doses plotted against $pIRIR_{150}$ D_e values for these samples (C).

The $IRSL_{50}$ and $pIRIR_{150}$ *g*-values for all discs are summarized as histograms in Fig. 9A. The mean $pIRIR_{150}$ *g*-value is 0.76±0.07%/decade and the relative standard deviation (rsd) is 78% ($n = 66$), which is much lower than the mean IR_{50} *g*-value of 3.00±0.08%/decade (rsd = 22%, $n = 66$). The average of six aliquots was calculated together with the standard error for each sample, which ranged between 2.1±0.9 and 3.7±0.9%/decade for the $IRSL_{50}$ and between 0.1±0.9 and 1.3±1.1%/decade for the $pIRIR_{150}$ (Fig. 9B; Table 4). The *g*-values for the pIRIR signal are significantly lower compared with the *g*-values of the IRSL, or even negligible. These results are similar for the $pIRIR_{150}$ signal of K-rich feldspar from young coastal sediments in Germany (Reimann & Tsukamoto 2012) and New Zealand (Madsen *et al.* 2011), although their $IRSL_{50}$ *g*-values were all above 5 %/decade. Thus, we propose that the use of the $pIRIR_{150}$ signal is able to reduce anomalous fading even to a negligible level, and so we used the D_e values (Fig. 3E, Table 4) derived from the $pIRIR_{150}$ signal for the luminescence age calculation.

Even though *g*-values of the $pIRIR_{150}$ signal for three of the 11 samples (e.g. ~1.0–1.5%/decade for samples NL-131, NL-134 and NL-136; this fading rate would predict age underestimation of ~10% or more) apparently suggest anomalous fading to a certain degree, there is no need to correct the $pIRIR_{150}$ ages for anomalous fading. This is because the laboratory fading experiments should not be considered as convincing evidence for loss of trapped charge during storage, especially for such low fading rates of 1.0–1.5%/decade; most likely these low apparent fading rates are an artefact of our measurement procedure, for instance because of inaccurate sensitivity correction after storage (Buylaert *et al.* 2012). In reality, even quartz samples, which are widely accepted to give stable signals on the time scales used here (Murray & Wintle 1999), can have mean *g*-values of 0.98±0.08%/decade (Buylaert *et al.* 2012). By comparison with an independent age control as well as quartz OSL ages, Reimann & Tsukamoto (2012) confirmed the accuracy of $pIRIR_{150}$ ages that were not corrected for anomalous fading. This further supports the suggestion above that

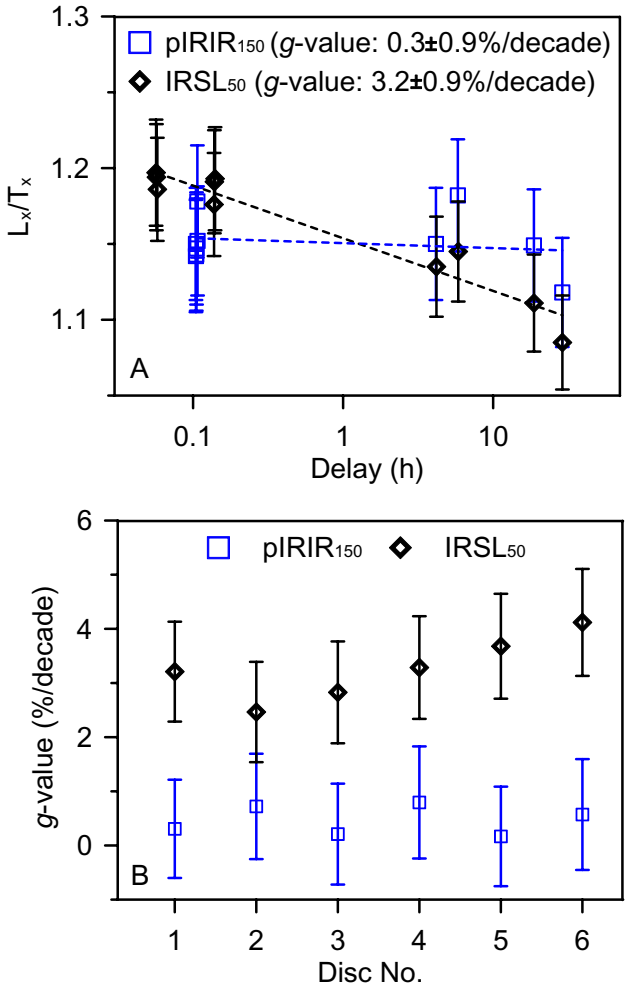

Fig. 8. Fading rate (*g*-value) determination of polymineral FG $IRSL_{50}$ and $pIRIR_{150}$ signals for a representative aliquot (A) and for six aliquots (B) of sample NL-130. This figure is available in colour at http://www.boreas.dk.

the $pIRIR_{150}$ signal should not be corrected for any apparent laboratory fading, and indicates that the measured (very low) fading rate for the $pIRIR_{150}$ signal may be a laboratory artefact, as suggested by Buylaert *et al.* (2011). Consequently, no fading correction was applied when using the $pIRIR_{150}$ D_e for age calculation.

Equivalent dose and age determination

For each sample 10–12 aliquots were used for each D_e measurement. All D_e estimates derived from the $pIRIR_{150}$ signal for the 11 samples are summarized in Table 4 and plotted against depth in Fig. 3E. After subtracting the residual doses the $pIRIR_{150}$ D_es were divided by dose rates derived from gamma spectrometry and NAA measurements to obtain luminescence ages (Table 4). As shown in Fig. 10, the two sets of luminescence ages are almost consistent with each other within errors. Surface samples, generally considered to be around zero age, can be used to check if dated sediments are fully bleached or insufficiently bleached prior to deposition. However, unfortunately our uppermost sediment sample (NL-129) yielded a significant age overestimation. This is not surprising because the dated material for this sample contains redeposited sediments of an assumed turbidite layer (2–5 cm sediment depth, grey bar in Fig. 10), which were identified macroscopically, as well as with magnetic susceptibility and grain-size analyses, although this was not evident during the sampling in the dark room. Turbidites are potential problems for luminescence dating (especially for the pIRIR signal) because they may not have received sufficient exposure to sunlight to reset the luminescence signal prior to burial. Turbidites undergo a rapid transport (Shanahan *et al.* 2013) and subaquatic relocation of the material within a lake is very likely. This assumption is confirmed by three other layers influenced by redeposition. Three additional samples (NL-135, NL-136 and NL-139) also include turbidite layers (Figs 1B, 10), resulting in age overestimations. Thus, the ages of these four samples containing turbidites were omitted from the luminescence data set to construct the age framework of sediment core TAN10/4 (Fig. 11). The ages of the remaining seven samples are in stratigraphical order within the uncertainties. By extrapolating a linear fit of these ages to the core top, we obtained a surface age that is close to zero (within uncertainty), implying a sufficient resetting of the used luminescence signal ($pIRIR_{150}$ signal) for dating and thus the applicability of our methods.

Comparison between $pIRIR_{150}$ and ^{14}C ages

The dose recovery test, a key screening test to check how suitable a chosen dating procedure is, suggested that our protocol is able to accurately measure doses given in the laboratory (see discussion above). However, this test can only inform about the reliability of laboratory-administered doses and behaviour, and cannot be used to assess the likelihood of accurately measuring the natural D_e (e.g. Roberts 2012). For this reason, it is important to be able to compare the dates generated using the pIRIR protocol against an independent age control (e.g. ^{14}C dating). Five radiocarbon ages from the studied sediment core were obtained, which are summarized in Table 5 and plotted against the depth scale in Fig. 11. Terrestrial plant macrofossils are well known to be most suitable for radiocarbon dating of lake sediments, as they are not affected by old carbon reservoir effects (Long *et al.* 2011), and the radiocarbon age of a wood fragment in one of the samples (lab ID: Beta-295005) may thus represent the timing of the corresponding deposition event. As shown in Fig. 11, the calibrated ^{14}C age of the wood sample (shown by blue diamond) lies on the regression

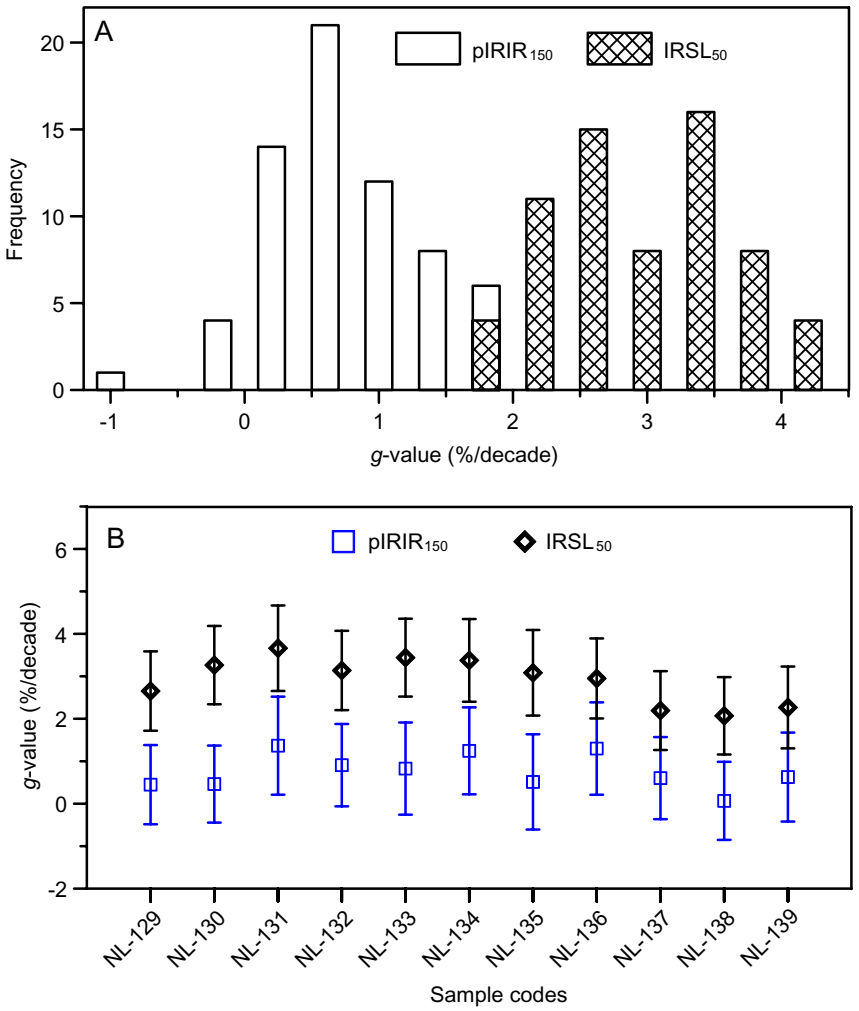

Fig. 9. A. Histogram summarizing $IRSL_{50}$ (unfilled) and $pIRIR_{150}$ (diagonal-cross filled) fading rates for all 11 samples (six aliquots for each sample). B. Comparison of average *g*-values of the 11 samples. This figure is available in colour at http://www.boreas.dk.

line (line A in Fig. 11) of pIRIR ages within errors, suggesting that the two dating techniques are in good agreement. Thus, the pIRIR ages and radiocarbon age of the wood sample are assumed to represent the best approximation for the depositional ages as no impact of old carbon on the ^{14}C dating of this wood sample is expected, further confirming the reliability of pIRIR dates of the current study.

For the data set of ^{14}C ages, except for the wood sample, the remaining ^{14}C ages are generally in

Table 4. Luminescence dating results (ages corrected for residual dose, but not for fading).

Sample	Sediment depth (cm)	g-value (%/decade)		$pIRIR_{150}$ D_e (Gy)	$pIRIR_{150}$ residual dose (Gy)	Residual corrected D_e (Gy)	Luminescence age (a)	
		$pIRIR_{150}$	$IRSL_{50}$				Model 1	Model 2
NL-129	0-8	0.40 ± 0.97	2.70 ± 0.88	19.47 ± 0.26	0.66 ± 0.06	18.81 ± 0.27	5860 ± 300	
NL-130	16-24	0.50 ± 0.96	3.30 ± 0.95	2.40 ± 0.07	0.59 ± 0.08	1.81 ± 0.10	520 ± 30	480 ± 40
NL-131	32-40	1.37 ± 1.09	3.70 ± 0.96	3.18 ± 0.09	0.46 ± 0.08	2.72 ± 0.11	910 ± 60	820 ± 60
NL-132	48-56	0.90 ± 1.05	3.10 ± 0.94	3.32 ± 0.10	0.41 ± 0.05	2.91 ± 0.11	990 ± 60	940 ± 60
NL-133	66-74	0.80 ± 1.10	3.40 ± 0.95	5.15 ± 0.08	0.43 ± 0.01	4.72 ± 0.08	1550 ± 80	1410 ± 90
NL-134	80-88	1.20 ± 1.11	3.40 ± 1.00	7.22 ± 0.09	0.41 ± 0.06	6.81 ± 0.11	2010 ± 100	1760 ± 120
NL-135	99-107	0.50 ± 1.12	3.10 ± 1.00	12.48 ± 0.12	0.45 ± 0.02	12.03 ± 0.12	3740 ± 180	
NL-136	112-120	1.30 ± 1.07	2.90 ± 0.94	12.90 ± 0.28	0.37+0.07	12.53 ± 0.29	4280 ± 220	
NL-137	128-136	0.60 ± 0.98	2.20 ± 0.93	9.03 ± 0.13	0.54 ± 0.08	8.49 ± 0.15	2700 ± 130	2210 ± 140
NL-138	146-154	0.07 ± 0.97	2.07 ± 0.94	9.14 ± 0.15	0.50 ± 0.02	8.64 ± 0.15	2880 ± 140	2370 ± 150
NL-139	155-162	0.60 ± 1.00	2.30 ± 0.99	34.30 ± 0.31	0.69 ± 0.06	33.61 ± 0.32	10 710 ± 500	

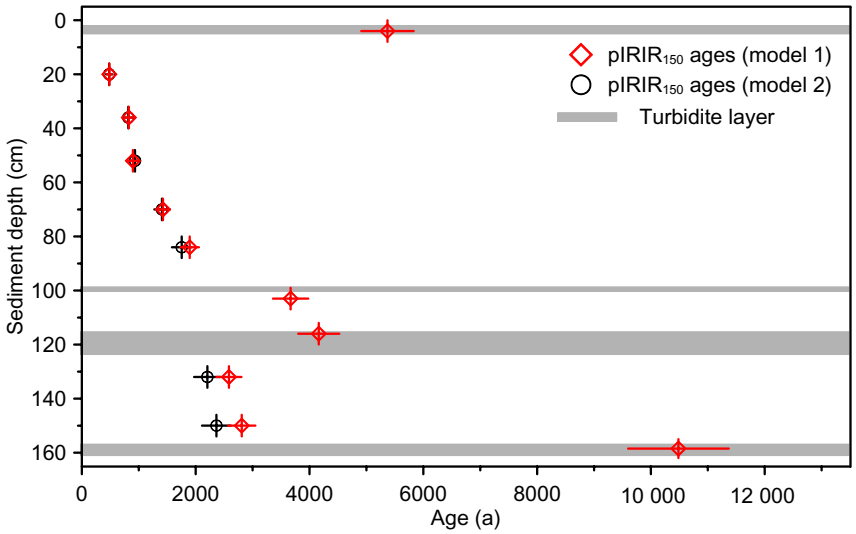

Fig. 10. All $pIRIR_{150}$ ages deduced from both models, which took into account uptake of U through time and loss of Th at deposition, respectively, for dose rate calculation. Grey band shows the location of four identified turbidite layers in the TAN10/4 core. This figure is available in colour at http://www.boreas.dk.

stratigraphical order, and these ages were used to construct a ^{14}C age-depth model by linear interpolation (dashed line B in Fig. 11). Obviously, there is a significant offset between both sets of age models, which suggests that the bulk organic-based ^{14}C ages are overall ~2 ka older than luminescence ages. Based on the robustness of luminescence dating for the TAN10/4 core, pIRIR ages are interpreted as directly indicating depositional ages. Accordingly, the age discrepancy between the luminescence and radiocarbon ages in this core probably results from the overestimation of radiocarbon ages, which is most likely caused by incorporation of old carbon. Thus, the offset between the two dating methods can be attributed to a reservoir effect. This interpretation is confirmed by the ^{14}C dates themselves because the surface sediments, which should contain modern carbon, have an age of 2140±30 a BP, giving evidence for a significant reservoir effect.

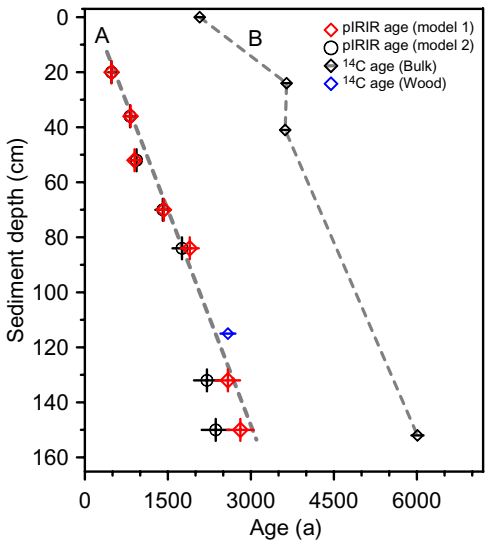

Fig. 11. Comparison of luminescence and radiocarbon dating based chronological frameworks. The pIRIR ages of four samples (i.e. NL-129, NL-135, NL-136 and NL-139), which apparently significantly overestimate age were not used, and the remaining seven samples' ages were used to construct the chronological framework. Dashed line A is the regression of these pIRIR dates derived from model 1. All calibrated ^{14}C ages are shown for comparison; one was derived from a wood sample (blue empty diamond), and the other four (denoted by black empty diamonds) were obtained using bulk organic matter (dashed line B). This figure is available in colour at http://www.boreas.dk.

Conclusions

Radioactive disequilibria in the uranium decay chain have been detected in lacustrine sediments from the Tangra Yumco. According to gamma spectrometry measurements, two models were used to account for the dynamic dose rates for age calculation. With regard to equivalent dose determination, we tested the applicability of a new pIRIR measurement protocol using polymineral FG to date deep-lake sediments from the Tibetan Plateau. Anomalous fading of this $pIRIR_{150}$ signal is negligible for the young samples studied, and thus the $pIRIR_{150}$ signal was used for dating the sediment core from Tangra Yumco. Turbidite deposition caused insufficient resetting of the pIRIR signal and thus apparent overestimation of four luminescence ages. However, the remaining luminescence data derived from the $pIRIR_{150}$ signal show ages in stratigraphical order, and their robustness is further confirmed by good agreement with the ^{14}C age of a woody (terrestrial) plant remain. Compared with the luminescence based age-depth model, ^{14}C dating generally yielded age overestimations, which may be attributable to hardwater reservoir effects in Tangra Yumco. As shown in this study, we emphasize that applying one single dating method is inappropriate for the lacustrine sediments for the TP, and thus multi-dating approaches are needed.

Table 5. Results of radiocarbon dating.

Lab ID (Beta-)	Sediment depth (cm)	Material	$\delta^{13}C$ (‰)	Age (a BP)	Age[1] (cal. a BP)	Converted age[2] (a)
295002	0	Bulk organic matter	–22.3	2140±30	2040–2160	2100–2220
295003	24	Bulk organic matter	–21.8	3450±40	3620–3830	3680–3890
295004	41	Bulk organic matter	–22.2	3410±40	3560–3730	3620–3790
295005	115	Wood	–24.5	2480±30	2450–2720	2510–2780
295006	152	Bulk organic matter	–22.3	5260±50	5920–6130	5980–6190

[1]The ^{14}C ages were calibrated to calendar years using the CALIB 6.1.0 program (Stuiver *et al*. 2011) with the internationally agreed IntCal09 data set (Reimer *et al*. 2009).

[2]The ^{14}C ages were adjusted to before 2010 (coring year) by plus 60 a for comparison with luminescence ages.

Acknowledgements. – Sabine Mogwitz (LIAG) is thanked for gamma spectrometry analysis. A special thanks is given to Wang Junbo (ITP CAS), who supported the fieldwork to retrieve the core with superior logistics and help during the coring campaign. Other helping hands from many Chinese and German colleagues in the field should be thanked as well. We are grateful to A. S. Murray, D. J. Huntley and J. A. Piotrowski for constructive comments, which led to significant improvement of this manuscript. This work was funded by the NSF of China (grant 41271002), the Strategic Priority Research Program (Climate Change: Carbon Budget and Relevant Issues) of the Chinese Academy of Sciences (grant XDA05120102), the 'NIGLAS 1–3-5 Project' (grant NIGLAS2012135004), the State Key Laboratory of Lake Science and Environment (grant 2012SKL002), the DFG Priority Programme 1372 (grant MA1308/23-2) and the China Postdoctoral Science Foundation (grant 2012M520061). Thomas Kasper particularly wishes to thank the 'Carl Zeiss Stiftung' for financial support of a PhD grant.

References

Aitken, M. J. 1985: *Thermoluminescence Dating*. 359 pp. Academic Press, London.

Auclair, M., Lamothe, M. & Huot, S. 2003: Measurement of anomalous fading for feldspar IRSL using SAR. *Radiation Measurements 37*, 487–492.

Bøtter-Jensen, L., Andersen, C. E., Duller, G. A. T. & Murray, A. S. 2003: Developments in radiation, stimulation and observation facilities in luminescence measurement. *Radiation Measurements 37*, 535–541.

Buylaert, J. P., Jain, M., Murray, A. S., Thomsen, K. J., Thiel, C. & Sohbati, R. 2012: A robust feldspar luminescence dating method for Middle and Late Pleistocene sediments. *Boreas 41*, 435–451.

Buylaert, J. P., Murray, A. S., Thomsen, K. J. & Jain, M. 2009: Testing the potential of an elevated temperature IRSL signal from K-feldspar. *Radiation Measurements 44*, 560–565.

Buylaert, J. P., Thiel, C., Murray, A. S., Vandenberghe, D. A. G., Yi, S. & Lu, H. 2011: IRSL and post-IR IRSL residual doses recorded in modern dust samples from the Chinese Loess Plateau. *Geochronometria 38*, 432–440.

Davids, F., Duller, G. A. T. & Roberts, H. M. 2010: Testing the use of feldspars for optical dating of hurricane overwash deposits. *Quaternary Geochronology 5*, 125–130.

Guérin, G., Mercier, N. & Adamiec, G. 2011: Dose-rate conversion factors: update. *Ancient TL 29*, 5–8.

Haberzettl, T., Anselmetti, F., Bowen, S., Fey, M., Mayr, C., Zolitschka, B., Ariztegui, D., Mauz, B., Ohlendorf, C., Kastner, S., Lücke, A., Schäbitz, F. & Wille, M. 2009: Late Pleistocene dust deposition in the Patagonian steppe – extending and refining the paleoenvironmental and tephrochronological record from Laguna Potrok Aike back to 55 ka. *Quaternary Science Reviews 28*, 2927–2938.

Hou, J., D'Andrea, W. J. & Liu, Z. 2012: The influence of ^{14}C reservoir age on interpretation of paleolimnological records from the Tibetan Plateau. *Quaternary Science Reviews 48*, 67–79.

Hua, Q. 2009: Radiocarbon: a chronological tool for the recent past. *Quaternary Geochronology 4*, 378–390.

Huntley, D. J. & Lamothe, M. 2001: Ubiquity of anomalous fading in K-feldspars and the measurement and correction for it in optical dating. *Canadian Journal of Earth Sciences 38*, 1093–1106.

Kasper, T., Haberzettl, T., Doberschütz, S., Daut, G., Wang, J., Zhu, L., Nowaczyk, N. & Mäusbacher, R. 2012: Indian Ocean Summer Monsoon (IOSM)-dynamics within the past 4 ka recorded in the sediments of Lake Nam Co, central Tibetan Plateau (China). *Quaternary Science Reviews 39*, 73–85.

Lamothe, M., Auclair, M., Hamzaoui, C. & Huot, S. 2003: Towards a prediction of longterm anomalous fading of feldspar IRSL. *Radiation Measurement 37*, 493–498.

Lang, A. & Zolitschka, B. 2001: Optical dating of annually laminated lake sediments: a test case from Holzmaar, Germany. *Quaternary Science Reviews 20*, 737–742.

Lee, J., Li, S.-H. & Aitchison, J. C. 2009: OSL dating of paleoshorelines at Lagkor Tso, western Tibet. *Quaternary Geochronology 4*, 335–343.

Lee, M. K., Lee, Y. I., Lim, H. S., Lee, J. I., Choi, J. H. & Yoon, H. I. 2011: Comparison of radiocarbon and OSL dating methods for a Late Quaternary sediment core from Lake Ulaan, Mongolia. *Journal of Paleolimnology 45*, 127–135.

Long, H., Lai, Z., Frenzel, P., Fuchs, M. & Haberzettl, T. 2012a: Holocene moist period recorded by the chronostratigraphy of a lake sedimentary sequence from Lake Tangra Yumco on the south Tibetan Plateau. *Quaternary Geochronology 10*, 136–142.

Long, H., Lai, Z., Fuchs, M., Zhang, J. & Li, Y. 2012b: Timing of Late Quaternary palaeolake evolution in Tengger Desert of northern China and its possible forcing mechanisms. *Global and Planetary Change 92–93*, 119–129.

Long, H., Lai, Z., Wang, N. & Zhang, J. 2011: A combined luminescence and radiocarbon dating study of Holocene lacustrine sediments from arid northern China. *Quaternary Geochronology 6*, 1–9.

Long, H., Shen, J., Tsukamoto, S., Chen, J. H., Yang, L. H. & Frechen, M. 2014: Dry early Holocene revealed by sand dune accumulation chronology in Bayanbulak Basin (Xinjiang, NW China). *The Holocene 24*, 614–626.

Lukas, S., Preusser, F., Anselmetti, F. S. & Tinner, W. 2012: Testing the potential of luminescence dating of high-alpine lake sediments. *Quaternary Geochronology 8*, 23–32.

Madsen, A. T. & Murray, A. S. 2009: Optically stimulated luminescence dating of young sediments: a review. *Geomorphology 109*, 3–16.

Madsen, A. T., Buylaert, J. & Murray, A. 2011: Luminescence dating of young coastal deposits from New Zealand using feldspar. *Geochronometria 38*, 378–390.

Madsen, A. T., Murray, A., Andersen, T. J., Pejrup, M. & Breuning-Madsen, H. 2005: Optically stimulated luminescence dating of young estuarine sediments: a comparison with ^{210}Pb and ^{137}Cs dating. *Marine Geology 214*, 251–268.

Madsen, D. B., Ma, H. Z., Rhode, D., Brantingham, P. J. & Forman, S. L. 2008: Age constraints on the late Quaternary evolution of Qinghai Lake, Tibetan plateau. *Quaternary Research 69*, 316–325.

Mischke, S., Weynell, M., Zhang, C. & Wiechert, U. 2013: Spatial variability of ^{14}C reservoir effects in Tibetan Plateau lakes. *Quaternary International 313–314*, 147–155.

Morthekai, P., Jain, M., Murray, A. S., Thomsen, K. J. & Bøtter-Jensen, L. 2008: Fading characteristics of martian analogue materials and the applicability of a correction procedure. *Radiation Measurement 43*, 672–678.

Mügler, I., Gleixner, G., Günther, F., Mäusbacher, R., Daut, G., Schütt, B., Berking, J., Schwalb, A., Schwark, L., Xu, B., Yao, T., Zhu, L. & Yi, C. 2010: A multi-proxy approach to reconstruct hydrological changes and Holocene climate development of Nam Co, Central Tibet. *Journal of Paleolimnology 43*, 625–648.

Murray, A. S. & Olley, J. M. 2002: Precision and accuracy in the optically stimulated luminescence dating of sedimentary quartz: a status review. *Geochronometria 21*, 1–166.

Murray, A. S. & Wintle, A. G. 1999: Isothermal decay of optically stimulated luminescence in quartz. *Radiation Measurements 30*, 119–125.

Murray, A. S. & Wintle, A. G. 2000: Luminescence dating of quartz using an improved single-aliquot regenerative-dose protocol. *Radiation Measurements 32*, 57–73.

Murray, A. S., Marten, R., Johnston, A. & Martin, P. 1987: Analysis for naturally occurring radionuclides at environmental concentrations by gamma spectrometry. *Journal of Radioanalytical and Nuclear Chemistry 115*, 263–288.

Murray, A. S., Thomsen, K. J., Masuda, N., Buylaert, J. P. & Jain, M. 2012: Identifying well-bleached quartz using the different bleaching rates of quartz and feldspar luminescence signals. *Radiation Measurements 47*, 688–695.

Olley, J. M., Murray, A. S. & Roberts, R. G. 1996: The effect of disequilibria in the uranium and thorium decay chains on burial dose rates in fluvial sediments. *Quaternary Science Reviews 15*, 751–760.

Preusser, F., Chithambo, M. L., Götte, T., Martini, M., Ramseyer, K., Sendezera, E. J., Susino, G. J. & Wintle, A. G. 2009: Quartz as a natural luminescence dosimeter. *Earth-Science Reviews 97*, 184–214.

Rades, E. F., Hetzel, R., Xu, Q. & Ding, L. 2013: Constraining Holocene lake-level highstands on the Tibetan Plateau by ^{10}Be exposure dating: a case study at Tangra Yumco, southern Tibet. *Quaternary Science Reviews 82*, 68–77.

Reimann, T. & Tsukamoto, S. 2012: Dating the recent past (<500 years) by post-IR IRSL feldspar- Examples from the North Sea and Baltic Sea coast. *Quaternary Geochronology 10*, 180–187.

Reimann, T., Tsukamoto, S., Naumann, M. & Frechen, M. 2011: The potential of using K-rich feldspars for optical dating of young coastal sediments – a test case from Darss-Zingst peninsula (southern Baltic Sea coast). *Quaternary Geochronology 6*, 207–222.

Reimer, P. J., Baillie, M. G. L., Bard, E., Bayliss, A., Beck, J. W., Blackwell, P. G., Bronk, R. C., Buck, C. E., Burr, G. S., Edwards, R. L., Friedrich, M., Grootes, P. M., Guilderson, T. P., Hajdas, I., Heaton, T. J., Hogg, A. G., Hughen, K. A., Kaiser, K. F., Kromer, B., McCormac, F. G., Manning, S. W., Reimer, R. W., Richards, D. A., Southon, J. R., Talamo, S., Turney, C. S. M., van der Plicht, J. & Weyhenmeyer, C. 2009: IntCal09 and Marine09 radiocarbon age calibration curves, 0–50,000 years cal BP. *Radiocarbon 51*, 1111–1150.

Roberts, H. M. 2012: Testing Post-IR IRSL protocols for minimising fading in feldspars, using Alaskan loess with independent chronological control. *Radiation Measurements 47*, 716–724.

Shanahan, T. M., Peck, J. A. & McKay, N. 2013: Age models for long lacustrine sediment records using multiple dating approaches-An example from Lake Bosumtwi, Ghana. *Quaternary Geochronology 15*, 47–60.

Stevens, T., Marković, S. B., Zech, M. & Sümegi, P. 2011: Dust deposition and climate in the Carpathian Basin over an independently dated last glacial-interglacial cycle. *Quaternary Science Reviews 30*, 662–681.

Stuiver, M., Reimer, P. J. & Reimer, R. W. 2011: CALIB Radiocarbon Calibration: downloadable programme and manual. Available at: http://calib.qub.ac.uk/calib/ (accessed 30.11.2011).

Thiel, C., Buylaert, J. P., Murray, A. S., Terhorst, B., Hofer, I., Tsukamoto, S. & Frechen, M. 2011: Luminescence dating of the Stratzing loess profile (Austria)-Testing the potential of an elevated temperature post-IR IRSL protocol. *Quaternary International 234*, 23–31.

Thomsen, K. J., Murray, A. S., Jain, M. & Bøtter-Jensen, L. 2008: Laboratory fading rates of various luminescence signals from feldspar-rich sediment extracts. *Radiation Measurements 43*, 1474–1486.

Tsukamoto, S., Jain, M., Murray, A. S., Thiel, C., Schmidt, E., Wacha, L., Dohrmann, R. & Frechen, M. 2012: A comparative study of the luminescence characteristics of polymineral fine grains and coarse-grained K- and Na-rich feldspars. *Radiation Measurements 47*, 903–908.

Walker, M. 2005: *Quaternary Dating Methods*. 286 pp. John Wiley & Sons, Ltd, Chichester.

Wang, J., Peng, P., Ma, Q. & Zhu, L. 2010: Modern Limnological features of Tangra Yumco and Zhari Namco, Tibetan Plateau. *Journal of Lake Science 22*, 629–632.

Wang, S. & Dou, H. 1998: *Lakes in China*. 580 pp. Science Publisher, Beijing (in Chinese).

Wintle, A. G. 1973: Anomalous fading of thermoluminescence in mineral samples. *Nature 245*, 143–144.